Multiple Scattering Properties Based on Modified Microsurface pBRDF Model

Youfei Hao, Jin Duan, Ju Liu, Jiahao Yang, and Juntong Zhan

***Abstract*—Scattering polarization properties are one of the main characteristics of a target. Different material types of the target surface can be expressed by the scattering polarization properties, and the use of polarization to characterise the target more effectively is a highly interesting topic. However, the existing polarized bidirectional reflection distribution function (pBRDF) based on microfacet theory for modelling light transmission over rough surfaces is not general. Modelling the scattering phenomena accurately on microsurfaces from a single specularly polarized reflection to full consideration of diffuse polarization remains a challenging task. In this work, we further introduce a directional diffuse reflection lobe to completely define the polarization properties of light in scattering, and revisit the microsurface in the masking and shadowing function part of the model, expanding the traditional symmetric V-groove structure, which is complemented by an asymmetric V-groove structure to improve the accuracy of the model description. We verify through a series of simulations and experiments that our model is in better agreement with the actual truth and that it is more suitable for describing the scattering polarization properties of most targets.**

***Index Terms*—Microfacet, polarized bidirectional reflection distribution function (pBRDF), polarization properties, scattering.**

I. Introduction

COMPARED with traditional detection technology, polarization detection technology can simultaneously obtain the target surface intensity information and polarization information. The acquisition of target polarization information effectively expands the information dimension and enhances the texture features to effectively improve the accuracy of target detection and identification. Therefore, polarization detection technology can be widely used in target detection [1], [2], medical diagnosis [3], [4] and military applications [5], [6], etc.

Manuscript received 17 August 2023; revised 7 September 2023; accepted 10 September 2023. Date of publication 12 September 2023; date of current version 21 September 2023. This work was supported in part by the Science and Technology Development Program of Jilin Province under Grant 20210203181SF, in part by the Science and Technology Development Program of Jilin Province under Grant 20220508152RC, and in part by the National Natural Science Foundation of China under Grant 62127813. *(Corresponding author: Jin Duan.)*

Youfei Hao, Ju Liu, and Jiahao Yang are with the Electronics, Information Engineering Institute, Changchun University of Science, Changchun 130022, China.

Jin Duan is with the Electronics, Information Engineering Institute, Changchun University of Science, Changchun 130022, China, and also with the Space Opto-Electronics Technology Institute, Changchun University of Science, Technology, Changchun 130022, China (e-mail: email:duanjin@vip.sina.com).

Juntong Zhan is with the Space Opto-Electronics Technology Institute, Changchun University of Science, Technology, Changchun 130022, China.

Digital Object Identifier 10.1109/JPHOT.2023.3314756

Polarization is a special information distinguished from visible light, which can be described by representations such as degree of polarization (DoP) and angle of polarization (AoP). Different targets or different states of the same target exhibit different polarization states. Normally, an ideal smooth surface would present significant polarization properties, but in practical measurements the target surfaces are rougher [7]. The polarization imaging of rough surfaces is influenced by physical factors such as refractive index and surface roughness of the target, so that the polarization imaging of the target can effectively distinguish between targets of different materials. Therefore, it is crucial to investigate the polarization reflection characteristics of rough surfaces of different materials.

To investigate the scattering properties of light, Nicodemus proposed the bidirectional reflection distribution function (BRDF), and subsequently many BRDF models based on geometrical optics were studied [8], [9], [10]. Among them, the Torrance-Sparrow model [11] and the Cook-Torrance model [12] are widely used. Aivar Abrashuly [13] suggested that the scattering in the visible spectrum needs to take into account their dispersive behavior. With the study of the polarization scattering properties of light, the effect of the masking effect is adequately considered. Wang et al. [34] developed a three-component polarimetric BRDF (pBRDF) model of specular reflection, diffuse reflection and body scattering to investigate the polarization properties of the target surface in response to the Blinn masking effect. Hyde IV et al. [14] developed a more accurate pBRDF model of the target surface based on the PG model [15] considering the masking effect and Lambert diffuse reflection. Zhan Hanyu et al. [16] modified the pBRDF model based on the Kubelka-Munk theory and derived the polarization model. The above studies on the properties of microfacet elements all make a strong assumption in essence: microfacets, defined as perfect mirror surfaces. However, it is well known that the target surface is not smooth and there are different masking and shadowing effects between neighboring surface elements. The existing simplified masking models such as Blinn approximates that the angles between adjacent face elements are equal, i.e., the surface is modeled as a symmetric V-groove cavity, which is not compatible with the actual rough surface situation, especially when dealing with general anisotropic materials such as Kulla and Conty [17]. In view of the above studies, it is urgent to explore the masking effect for more closely matching the actual rough surfaces. Inspired by the literature [18], we develop a closed-form of multiple analysis microfacet shading and masking function that takes into

account the additional scattering that occurs again after the first scattering and without a significant increase in computational effort. We treat the microfacet when polarized scattering of light occurs as a symmetric V-groove structure and an asymmetric V-groove structure, and calculate the multiple scattering that occurs therein. The introduction of the asymmetric V-groove structure increases the degrees of freedom in the representation of the microfacet and allows a better description of the reflections arising at the grazing angle, especially for describing metallic materials.

All modifications are made to improve the applicability of pBRDF. The pBRDF models consist of a combination of roughly polarized specular lobe (Fresnel interactions in microsurface models) and depolarized diffuse reflection lobe [19], [20], [21] to consider diffuse reflection polarization effects [22]. In addition to specular surface reflectance lobe and diffuse reflection lobe, which are considered in most models, it has been shown that the reflection of light also includes directional diffuse reflection lobe [23]. In the study of polarization properties, the polarization effects produced by all reflection lobes should not be neglected. Zhu et al. [24] successfully introduced the directional diffuse reflection lobe into the polarimetric BRDF. To accurately describe the polarization properties of surface scattering, we also refer to the recent results of Jianfeng Sun et al. [25] and introduce the directional diffuse reflection component that distinguishes them for a complete analysis of the model, making the model more reliable overall.

II. Theoretical Simulation

A. Basic Concept

In order to graphically describe the reflection properties of the object surface for different incident illumination at arbitrary observation angles, Nicodemus [26] was the first to propose the bidirectional reflection distribution function (BRDF) model, which was defined as the ratio of the reflected radiance to the radiant irradiance of the incident illumination, i.e:

$$f_{BRDF}\left(\theta_i, \varphi_i, \theta_r, \varphi_r\right) = \frac{dL_r\left(\theta_i, \varphi_i, \theta_r, \varphi_r\right)}{dE_i\left(\theta_i, \varphi_i\right)} \tag{1}$$

θ and φ are the zenith and azimuth angles, respectively. Subscript i and r represent the direction of incidence and reflection, respectively.

To study the effect of microscopic distribution of rough surfaces on the polarization characteristics of objects, the scalar microsurface bidirectional reflection distribution function is vectorized to form the polarimetric BRDF (pBRDF), which can be expressed as:

$$F_{pBRDF}\left(\theta_i, \varphi_i, \theta_r, \varphi_r, \lambda\right) = \frac{dL_r\left(\theta_i, \varphi_i, \theta_r, \varphi_r, \lambda\right)}{dE_i\left(\theta_i, \varphi_i, \lambda\right)} \tag{2}$$

Where, $dL_r(\theta_i, \varphi_i, \theta_r, \varphi_r, \lambda)$ is the Stokes vector of scattered radiation from the target surface and $dE_i(\theta_i, \varphi_i, \lambda)$ is the Stokes vector of incident radiation. F is a 4×4 Muller matrix. The reflection scattering phenomenon of illumination on the micro-element surface of the target is shown in Fig. 1.

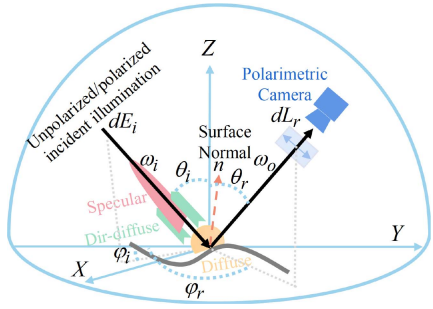

Fig. 1. Schematic diagram of the bi-directional reflection distribution function model for micro-elements, $\varphi_v = \varphi_r - \varphi_i$ is the relative azimuthal angle.

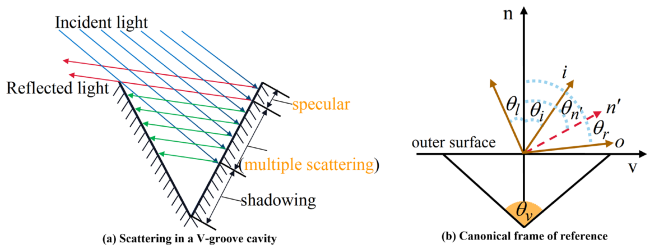

Fig. 2. Schematic diagram of shading and masking phenomena: (a) V-groove structure; (b) canonical reference system, where the angle of the slot $\theta_v = |\pi + \theta_l - \theta_r|$.

III. The Shading and Masking Function for Multiple Scattering

The phenomenon of incident illumination not being completely reflected on a microfacet element due to the concavity of the microfacet element is called masking. In order to accurately describe the reflection scattering phenomenon of light rays on rough surfaces, shading and masking functions are proposed, which are determined by the masking and masking probabilities of reflections from neighboring surface elements [27]. To unify the description, the reference system of the V-groove structure is specified, and the incident ray i and the reflected ray r can be mapped to the $n - s$ plane.

Inspired by the literature [9], we use a kaleidoscope model for the construction of multiple scattering. In order to be able to describe the microfacet elements accurately, the adjacent surface elements are divided into two categories: symmetric V-groove structures and asymmetric V-groove structures. In different structures, the numbers of scattering will be presented in different forms, which can be described in the form of linear equations, as shown in Figs. 3 and 4. Among them, Figs. 3(a) and 4(a) depict the multiple scattering in symmetric V-groove structure and asymmetric V-groove structure, respectively, and Figs. 3(b) and 4(b) show examples of geometric attenuation.

As shown in Figs. 3 and 4, the symmetric V-groove has an isosceles triangular structure, and the circle passing through the two most edge points of the V-groove can be obtained with its waist length; while the asymmetric V-groove obtains a concentric circle with two different waist lengths. We only need to determine the number of reflections occurring by judging the number of intersections of the line with the circle in question. When $k = 1$, the incident illumination undergoes

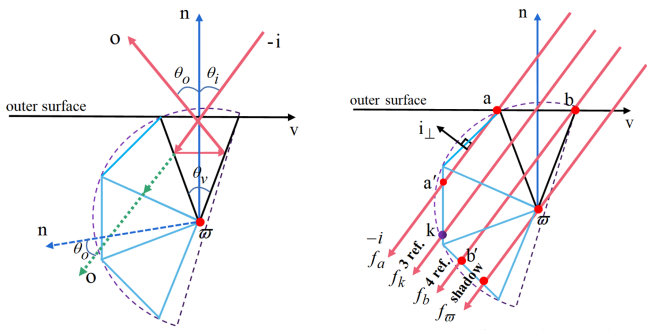

(a) Multi-scatting in a symmetric V-groove

(b) An example of geometric attenuation inside the symmetric V-groove.

Fig. 3. Kaleidoscope reflection model description of multiple reflections within a symmetric V-groove structure: (a) multiple scattering in a symmetric V-groove structure; (b) an example of geometric attenuation inside the symmetric V-groove with three and four bounces, respectively. Where, k represents the number of reflections of the incident light.

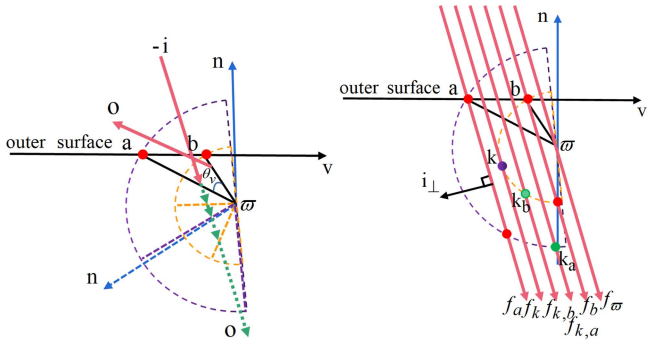

(a) Multi-scatting in a nonsymmetric V-groove

(b) An example of the geometric attenuation inside the nonsymmetric V-groove

Fig. 4. Kaleidoscope reflection model description of multiple reflections within a nonsymmetric V-groove structure: (a) multiple scattering in a nonsymmetric V-groove structure; (b) an example of geometric attenuation inside the nonsymmetric V-groove with single scattering, two, three, and four bounces, respectively.

specular reflection or specular-like reflection phenomenon, and when $k > 1$, the scattered reflection phenomenon of incident illumination is diffuse reflection. Therefore, we can specify the specific reflection state in multiple scattering, i.e., the number of reflections k and the geometric term $G(\theta_i, \theta_r, \theta_v)$, based on the angle and position of the incident illumination. The equation of the line parallel to the direction of incidence i is $f(p) = i_\perp \cdot p$, where p denotes any point, and the output value of the function f denotes the orthogonal offset of the line from the origin ϖ. The geometric term $G(\theta_i, \theta_r, \theta_v)$ when multiple scattering occurs in a symmetric V-groove structure can be described as:

$$G\left(\theta_i, \theta_r, \theta_v\right) = \begin{cases} \left|f_a - f_k\right| / f_a & (k-1) \text{ reflections} \\ \left|f_b - f_k\right| / f_a & (k) \text{ reflections} \end{cases} \tag{3}$$

Fig. 3(a) depicts the multiple scattering phenomenon at $k = 3$ or 4, the different regions represent different scattering states.

Extending the kaleidoscope model to an asymmetric V-groove structure in which multiple scattering occurs the geometric term $G(\theta_i, \theta_r, \theta_v)$ can be described as (4) shown at the bottom of this page. Among them, $k_b = 2[2(\pi + \theta_i - \theta_r) - \theta_v / 2\theta_v + 0.5]$, $k_a = k_b + 1$ and $f_j = \min(f(j), 1)$.

A. A Modified Multiple Scattering pBRDF Model

The construction of pBRDF models usually follows the microfacet theory [28], [29], and most of them treat the scattering of incident illumination at the surface as a combination of two lobes with diffuse and specular reflections [30]. However, Baek et al. [31] suggested that the combination of two lobes is not consistent with the actual incident illumination scattering phenomenon. The actual reflection of incident illumination consists of three lobes, including a surface flap containing a "specular-cusp" lobe, i.e., surface reflection, and a wider specular surface reflection lobe, i.e., directional diffuse reflection. In general, specular spike lobe is particularly important for reflections from smooth surfaces, while rough surfaces require directional diffuse reflections to more completely characterize them. Guided by the ideas in the literature [25], we introduce a new additional term of directional diffuse reflection effect in the construction of the pBRDF model. As shown in Fig. 2, we define the scattering of incident illumination as specular reflection, diffuse reflection and directional diffuse reflection. Thus, the pBRDF can be completely represented as a sum of three components, described as:

$$F = F^s + F^d + F^{dd} \tag{5}$$

where F^s, F^d and F^{dd} denote the specular reflection lobe, diffuse reflection lobe and directional diffuse reflection lobe of the pBRDF, respectively.

1) Specular Reflection Lobe F^s: In the existing pBRDF model about specular reflection is more accurately described, according to the microfacet theory, the material surface can be considered as an infinite number of microfacet planes obeying Fresnel's reflection law and Gaussian distribution [32]. Its expression can be expressed as follows:

$$\begin{aligned} \boldsymbol{F}^s_{k,j}(\theta_i, \varphi_i, \theta_r, \varphi_r) &= \rho_s \frac{G(\theta_i, \theta_r, \theta_v)\mathrm{D}(\theta_h, \sigma)}{4\cos\theta_i \cos\theta_r} \\ M_{k,j}\left(\theta_i, \varphi_i, \theta_r, \varphi_r\right), (\mathrm{k}, \mathrm{j} &= 0, 1, 2, 3) \end{aligned} \tag{6}$$

where σ is the surface roughness parameter, ρ_s is the surface reflectance, G is the shading and masking function of multiple scattering, and $M_{k,j}(\theta_i, \varphi_i, \theta_r, \varphi_r)$ is the Fresnel reflectance Mueller matrix, which can be calculated by deriving the Jones

$$G\left(\theta_i, \theta_r, \theta_v\right) = \begin{cases} \max\left(0, f_a - \max\left(f_k, f_b\right)\right) / f_a & 1 \text{ reflections} \\ \max\left(0, \min\left(f_a, f_k\right) - f_{k,b}\right) / f_a & (k_b - 1) \text{ reflections} \\ \max\left(0, \min\left(f_a, f_{k,b}\right) - \max\left(f_b, f_{k,a}\right)\right) / f_a & k_b \text{ reflections} \\ \max\left(0, \min\left(f_{k,a}, f_{k,b}\right) - f_b\right) / f_a & (k_b + 1) \text{ reflections} \end{cases} \tag{4}$$

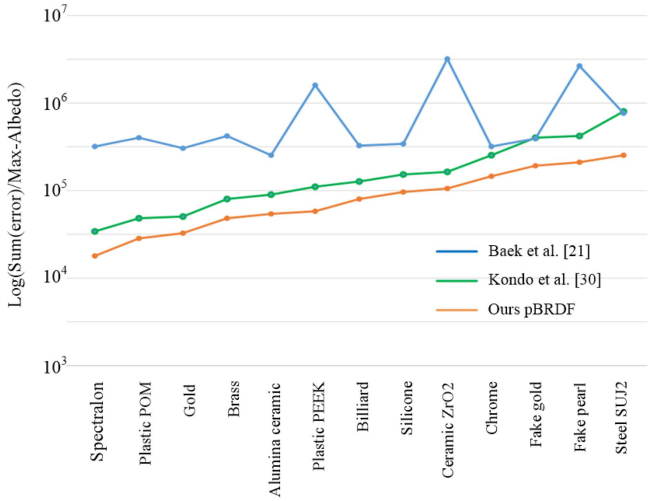

Fig. 5. Comparison of simulation errors for 13 materials:[21], [30] and our pBRDF. x-axis is the sum of fitting errors for each material and y-axis is the sum of fitting errors for reference [8]. The results were ranked according to the errors.

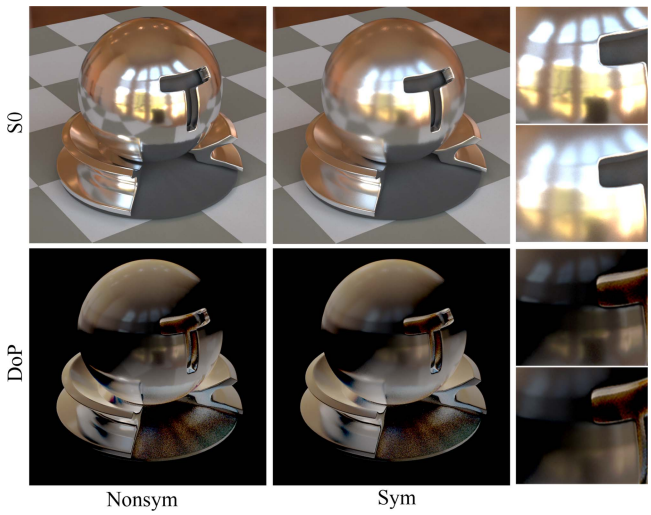

Fig. 6. Comparison of asymmetric (left) and symmetric (right) V-groove multiple scattering pBRDFs. The first row is the intensity comparison and the second row is the degree of polarization (DoP) comparison.

matrix, described as:

$$\begin{bmatrix} M_{00} \\ M_{10} \\ M_{20} \\ M_{30} \end{bmatrix} = \frac{1}{2} \begin{bmatrix} R_s + R_p \\ \cos(2\eta_r)(R_s - R_p) \\ \sin(2\eta_r)(R_p - R_s) \\ 0 \end{bmatrix} \tag{7}$$

From the description of (9), it can be found that the elements in the Fresnel reflectance Muller matrix are mainly determined by the complex refractive index (Fresnel reflectance) of the material.

2) Diffuse Reflection Lobe F^d: Diffuse reflection from object surface is caused by the incident radiation passing through multiple reflections between large adjacent angles and the body scattering inside the material. The radiation intensity of the diffuse reflection is usually expressed according to the Lambertian model. Therefore, the diffuse reflection is considered to be unpolarized, but this causes errors for the reflected radiation of most materials. X. Li et al. [33] corrected the diffuse reflection expression and applied the Lambertian microfacet to the integral of the macrofacet diffuse reflection. Thus, the diffuse reflection component can be defined as:

$$\boldsymbol{F}^d_{k,j}(\theta_i, \varphi_i, \theta_r, \varphi_r) = \rho_d \frac{G}{\pi} [C_1 + C_2(\frac{\sin\theta_i \sin\theta_r \cos\varphi_v}{\cos\theta_i \cos\theta_r})]$$

$$M^{\mathrm{d}}_{k,j}(\theta_i, \varphi_i, \theta_r, \varphi_r), (\mathrm{k,j} = 0, 1, 2, 3) \tag{8}$$

Where, ρ_d represents diffuse albedo, which can be expressed as the ratio of the total diffuse flux scattered inside the material to the incident radiation flux on the material surface. $C_1 = 0.8532\sigma^{-0.095}$, $C_2 = 0.3595\sigma^{1.785}$. Diffuse scattering is usually considered as an unpolarized phenomenon, therefore, is a depolarized Mueller matrix $M^d_{k,j}$:

$$\boldsymbol{M}^d_{k,j} = \begin{bmatrix} 1 & \cdots & 0 \\ \vdots & \ddots & \vdots \\ 0 & \cdots & 0 \end{bmatrix} \tag{9}$$

3) Directional Diffuse Reflection Lobe F^{dd}: The complete definition of polarized reflection is crucial for the pBRDF model to accurately describe the polarization properties of the material surface. In order to make the model fit better with the captured data, we introduce a new directional diffuse reflection term to extend the pBRDF model. The directional diffuse reflection term refers to the reflection phenomenon of incident radiation occurring within a microsurface with a large slope angle, and its energy mainly originates from a small reflection direction near the surface normal direction. Therefore, the energy of directional diffuse reflection is inversely proportional to the reflection angle. Thus, we can simply define the directional diffuse reflection lobe F^{dd}:

$$\boldsymbol{F}^{dd}_{k,j}(\theta_i, \varphi_i, \theta_r, \varphi_r) = \rho_{dd} \frac{1}{\sqrt{2\pi}\sigma} \exp\left(-2\tan\theta_r/\sigma^2\right)$$

$$M^{dd}_{k,j}(\theta_i, \varphi_i, \theta_r, \varphi_r), (\mathrm{k,j} = 0, 1, 2, 3) \tag{10}$$

where ρ_{dd} denotes the directional diffuse reflectance, which is a color vector, as opposed to the single-valued specular component. Since the directional diffuse reflection is generally generated on each wave lobe around the specular reflection, it exhibits a polarization state similar to that of the specular reflection. Therefore, $M^{dd}_{k,j}(\theta_i, \varphi_i, \theta_r, \varphi_r)$ can also be expressed by the Fresnel reflection Muller matrix, i.e. $M^{dd}_{k,j}(\theta_i, \varphi_i, \theta_r, \varphi_r) = M_{k,j}(\theta_i, \varphi_i, \theta_r, \varphi_r)$. Thus, combining the above expressions for each component, the modified multiple scattering pBRDF model is expressed as (11) shown at the bottom of the next page.

B. DoP Expression

In case the incident illumination is unpolarized light can be expressed in terms of stokes vectors as $S^{in} = [\ 1 \quad 0 \quad 0 \quad 0\ ]^T$. The Stokes vector of reflected light can be expressed as (12) shown at the bottom of the next page. Thus, the expression for DoP is defined as (13) shown at the bottom of the next page.

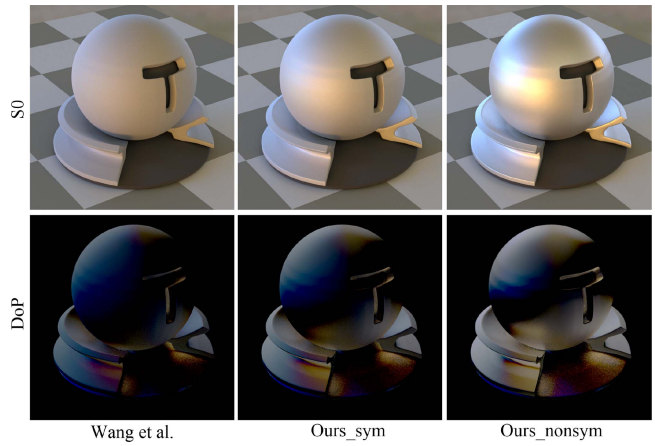

Fig. 7. Qualitative comparison between the results of Wang et al. and our model for an aluminum geometry with roughness $\alpha = 1.0$. Due to the different underlying microgeometry model, the appearance of multiple scattering differs significantly.

IV. Experiment Results and Analysis

A. pBRDF Model Accuracy Verification

To verify the superiority of the multiple scattering pBRDF model, we use a combination of genetic algorithm and least squares algorithm to obtain the optimal parameters by finding the mean minimum standard deviation of the simulated values of the model from the experimental measurements. The specific expression of the mean minimum standard deviation is given in the following equation.

$$\nabla E(n,k) = \min\left\{\sqrt{\left\{\frac{LY_{i=1}\left(Y_{\text{fit}}(i) - Y_{\text{measure}}(i)\right]^2}{L}\right\}}\right\} \tag{14}$$

TABLE I
Intrinsic Parameters of Different Material Surfaces Estimated Using Our Model

parameter	σ	η_{ours}	η_{GT}
alumina	0.2153	1.782	1.75-1.80
iron	0.1764	3.186	3.18-3.19
glass	0.12	1.529	1.52-1.53
PVC	0.3796	1.588	1.52-1.55

$\min\{\bullet\}$ denotes the calculated function of the minimum standard deviation, Y_{fit} denotes the model fit value, Y_{measure} denotes the experimental data captured by the measurement, and L is the total data volume.

For the optimal parameter estimation, we choose the measurement data with an incidence angle of 60° and an exit angle of $0^\circ - 60^\circ$ at 550 nm band to fit the best intrinsic material parameters (roughness σ and refractive index η). As shown in Table I, the estimates of refractive indices for the four common materials are within the range of ground truth, which also indicates the high accuracy of our method.

To further verify the validity and accuracy of our proposed model. In combination with Stokes-Muller imaging, we multiply the modeled Mueller matrix by various Stokes vectors to calculate the output vectors, which are then converted to luminance images after obtaining the output Stokes vectors. Finally, the accuracy of the model is evaluated by calculating the error between the simulated obtained luminance values and the reference values. Where the reference value is the publicly available KAIST pBRDF database [31], Fig. 5 shows the error statistics for the simulations of 13 different materials using [21], [30] and our pBRDF, respectively. From the graphical results, it is found that our model has a small error, which also indicates its ability to describe the polarization properties of different materials excellently.

$$\begin{aligned}\mathrm{F}_{k,j}(\theta_i,\theta_r,\varphi_v) &= \rho_s \frac{G(\theta_i,\theta_r,\theta_v)\,\mathrm{D}(\theta_h,\sigma)}{4\cos\theta_i\cos\theta_r} M^s_{k,j}(\theta_i,\varphi_i,\theta_r,\varphi_r) + \rho_d \frac{G(\theta_t,\theta_r,\theta_v)}{\pi}\left[C_1 + C_2\left(\frac{\sin\theta_i\sin\theta_r\cos\varphi_v}{\cos\theta_i\cos\theta_r}\right)\right] \\ &\quad M^{\mathrm{d}}_{k,j}(\theta_i,\varphi_i,\theta_r,\varphi_r) + \rho_{dd}\frac{1}{\sqrt{2\pi}\sigma}\exp\left(-2\tan\theta_r/\sigma^2\right) M^{dd}_{k,j}(\theta_i,\varphi_i,\theta_r,\varphi_r)\end{aligned} \tag{11}$$

$$\begin{aligned}S^{\text{out}} = F_{k,j}\cdot S^{in} &= \begin{bmatrix} F^s_{00}+F^d_{00}+F^{dd}_{00} & F^s_{01}+F^{dd}_{01} & F^s_{02}+F^{dd}_{02} & F^s_{03}+F^{dd}_{03} \\ F^s_{10}+F^{dd}_{10} & F^s_{11}+F^{dd}_{11} & F^s_{12}+F^{dd}_{12} & F^s_{13}+F^{dd}_{13} \\ F^s_{20}+F^{dd}_{20} & F^s_{21}+F^{dd}_{21} & F^s_{22}+F^{dd}_{22} & F^s_{23}+F^{dd}_{23} \\ F^s_{30}+F^{dd}_{30} & F^s_{31}+F^{dd}_{31} & F^s_{32}+F^{dd}_{32} & F^s_{33}+F^{dd}_{33} \end{bmatrix}\begin{bmatrix}1\\0\\0\\0\end{bmatrix} \\ &= \begin{bmatrix} F^s_{00}+F^d_{00}+F^{dd}_{00} \\ F^s_{10}+F^{dd}_{10} \\ F^s_{20}+F^{dd}_{20} \\ F^s_{30}+F^{dd}_{30} \end{bmatrix}\end{aligned} \tag{12}$$

$$\begin{aligned}DoP &= \frac{\sqrt{\left(F^s_{10}+F^{dd}_{10}\right)^2+\left(F^s_{20}+F^{dd}_{20}\right)^2}}{F^s_{00}+F^d_{00}+F^{dd}_{00}} \\ &= \frac{\sqrt{\left(\rho_s^2\frac{G^2D^2}{16\cos^2\theta_i\cos^2\theta_r}+\rho_s\rho_{dd}\frac{GD}{2\sqrt{2\pi}\cos\theta_i\cos\theta_r\sigma}+\rho_{dd}^2\frac{\exp[-(4\tan^2\theta_r)/\sigma^4]}{2\pi\sigma}\right)(M^2_{10}+M^2_{20})}}{M_{00}\left(\rho_s\frac{GD}{4\cos\theta_i\cos\theta_r}+\rho_{dd}\frac{\exp[-(2\tan\theta_r)/\sigma^2]}{\sqrt{2\pi}\sigma}\right)+\frac{\rho_d}{\pi}G\left(C_1+C_2\frac{\sin\theta_i\sin\theta_r\cos\varphi_v}{\cos\theta_i\cos\theta_r}\right)}\end{aligned} \tag{13}$$

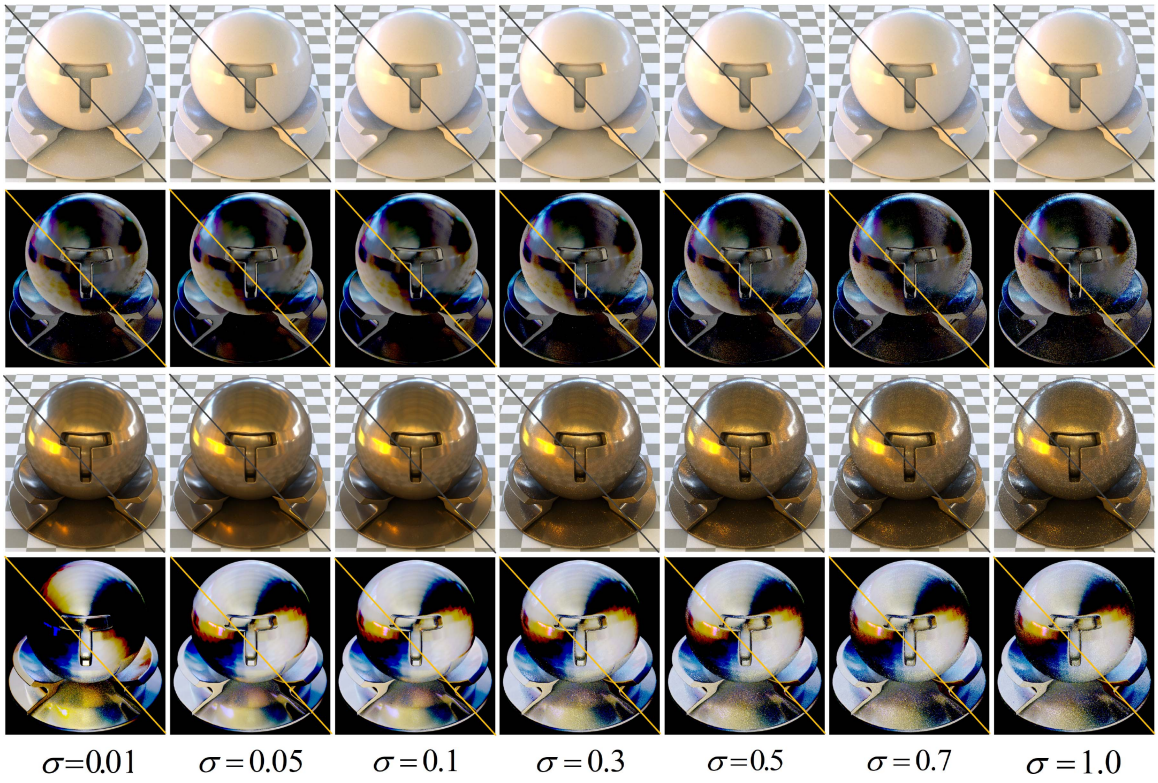

Fig. 8. Compare the intensity and DoP of the multiple scattering shading and masking function model (top right) with the literature [35] (bottom left) for two materials with different roughness.

B. Evaluation

1) Symmetric vs. Nonsymmetric: In contrast to the traditional symmetric V-groove model, the introduction of the asymmetric V-groove provides a more accurate description of the light-material interaction. Fig. 6 compares the multiple scattering pBRDFs for symmetric and asymmetric V-grooves. The asymmetric V-groove model describes the micro-surface more closely to the real target surface, and it is able to characterize the scattering polarization state of the light from the target surface uniformly. On the contrary, the symmetric V-groove model shows specular polarization reflection attenuation, i.e., energy loss, for the concave parts of the target surface due to its singularity. This is reflected in a lower DoP. In addition, the asymmetric V-groove model produces more backward scattering due to the consideration of the multiple scattering of light.

2) Comparison With Wang et al. [34]: The main difference between the work of Wang et al. and ours is the microsurface modeling: each microsurface produces a different type of multiple scattering.Wang et al. describes single scattering results. In contrast, the application of asymmetric V-grooves enables the model to describe the multiple scattering occurring on the surface with a finite number of descriptions. We compare these two models in Fig. 7, and the results reveal that our model is able to more accurately characterize the scattering of light from the target surface.

C. Validation

1) Shading and Masking Function Verifications: In order to verify the effectiveness of the multiple scattering shading and masking functions, we apply the model in mistuba 3 as a novel pBRDF to reproduct the object surface. Specifically, we use the polarization rendering mode to simulate polarized images of different materials (each with resolution 500×500). In polarization rendering mode, the renderer will track the polarization state of the light during the simulation. The system configuration reflects our real experimental setup. We use multiple scattering shading and masking function and the original symmetric shading and masking function [35] to simulate polarized surface. We perform tests on various 3D models and surface reflectivity. Fig. 8 shows the intensity and polarization images of two kinds of materials plastic POM and brass with different roughness affixed to the material text ball. Where, the first and second rows indicate the intensity and DoP of plastic POM after rendering, respectively. The third and fourth rows represent the intensity and DoP of brass after rendering, respectively. Here, we divide the scene into the top right and the bottom left, representing the rendering results of the multiple scattering shading and masking function and the original symmetric shading and masking function, respectively.

2) Shading and Masking Function Verifications: The surface roughness is an important parameter to control the parametric pBRDF model, and the original symmetric shading and masking functions do not take into account the effects generated by multiple scattering caused with increasing roughness. Especially when the roughness value is high, the symmetric shading and masking functions will omit more specular reflections, resulting in energy loss from the object surface, which will also lead to a darker intensity after rendering. On the contrary, for multiple scattering shading and masking functions that consider

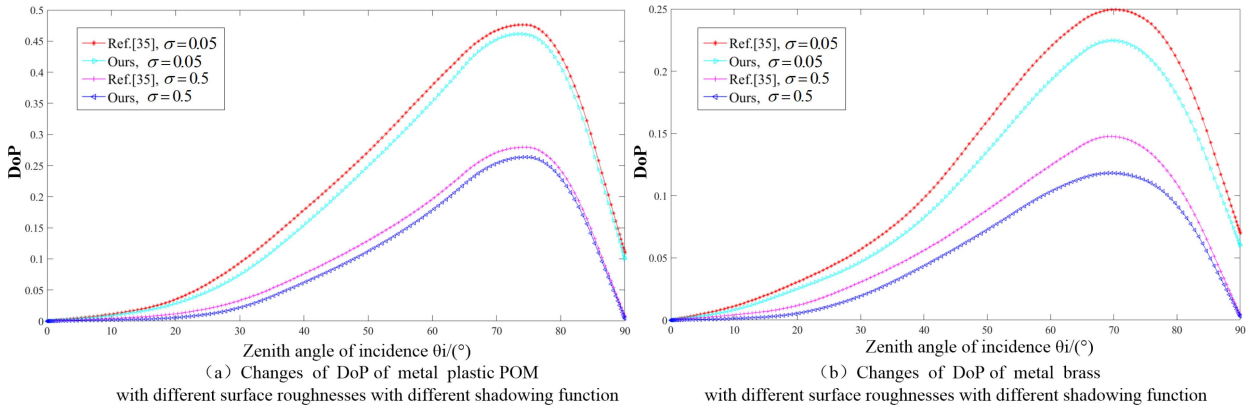

（a）Changes of DoP of metal plastic POM with different surface roughnesses with different shadowing function

（b）Changes of DoP of metal brass with different surface roughnesses with different shadowing function

Fig. 9. DoP obtained for plastic POM and brass using different shading and masking functions with roughness $\sigma = 0.05$ and $\sigma = 0.5$.

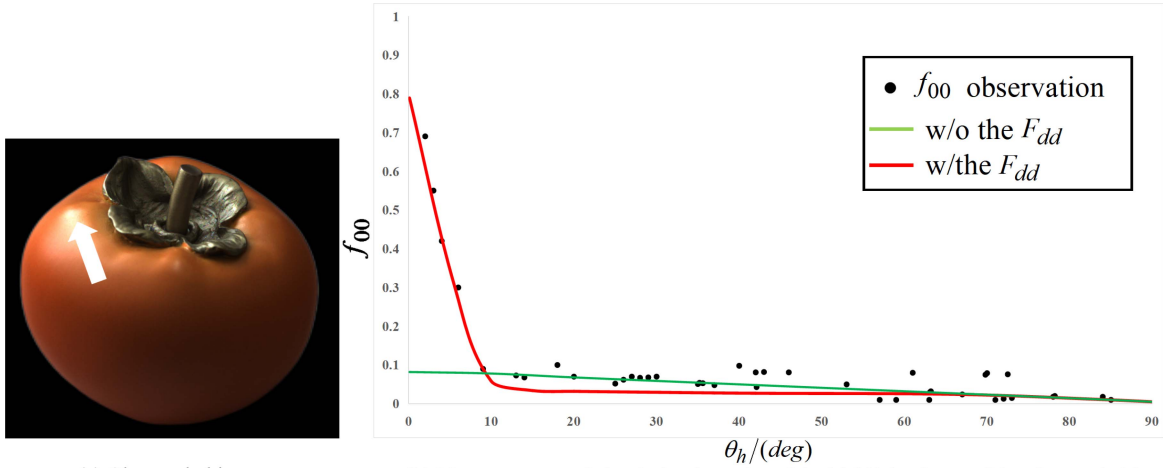

(a) Observed object

(b) Measurement and simulation intensity of the highlighted part of the observed object

Fig. 10. Intensity measurement of the object compared with the simulation. (a) The observed intensity values in the highlighted area without specular reflection intensity indicated by the arrow in the example image correspond to the black origin of the distribution in Fig. 10(b). (b) Intensity values obtained with the simulation of the model with or without the introduction of directional diffuse reflection lobe (red and green lines).

asymmetric structures, the difference in the object surface after rendering is tiny because they consider more variations in microsurface. When the surface roughness is less than 0.1, the normal dependence of the magnitude of DoP on the roughness is more obvious. Conversely, at higher surface roughness, this dependence will be abnormal and there will be a large difference in the polarization variation between metals and nonmetals. When the roughness is low, the plastic surface is smoother and its small scattering of incident illumination will make the object reflect higher DoP. However, when the roughness becomes larger, it will present a sparse and porous surface with a high proportion of diffuse reflection will make the DoP appear more varied. In contrast, the reflected light of metallic copper is mostly single scattered light, and the dispersion of DoP is relatively weak. Therefore, metal has a better deflection-preserving effect at high roughness compared to the dielectric material.

Fig. 9 shows a quantitative comparison of the DoP obtained for plastic POM and brass using different shading and masking functions with roughness $\sigma = 0.05$ and $\sigma = 0.5$. From this, it can be observed that there is a significant difference between the multiple scattering shading functions and the literature [35], especially in the range of incidence angles at the peak. The reason for this phenomenon is that at the same incident angle, the multiple scattering shading and masking functions take into account more carefully the scattering of the incident light on the surface and inside the object, thus providing an attenuation of the light and making the corresponding DoP lower. Comparing the differences of DoP under the two roughnesses, it is found that the larger the surface roughness, the more obvious the masking effect brought by the multiple scattering shadows and the masking function. Therefore, our masking function is of great importance for the accuracy of the rough surface model.

3) Influence of Directional Diffuse Lobe on Mirror Enhancement: Next, to evaluate the effect of the introduced directional diffuse reflection lobe on the specular enhancement, we analyze the intensity value f_{00} of the observed object. As Fig. 10(a) shows the observed target, there is almost no specular reflection at the point indicated by the arrow. The scatter in Fig. 10(b) indicates the intensity measurements of object. The green line shows the results of the simulation considering only specular reflections and the diffuse reflection model, and the red line indicates the results of our optimization after introducing the

directional diffuse reflection enhancement model. The results show that the model with the introduction of directional diffuse reflection can restore the missing specular information at a small angle and better fit the sparse captured data.

V. Conclusion

In order to extend the applicability of the polarimetric BRDF model to describe the polarization properties of materials, we propose a complete pBRDF model to serve the identification and classification of materials by taking into account the polarization of specular reflection, diffuse reflection and directional diffuse reflection. To deal with the microscale appearance of the target surface more accurately, we extend the traditional symmetric V-groove structure and consider the asymmetric V-groove structure in the construction of the masking and shadowing functions for the pBRDF model. The good agreement between the simulated DoP and measured DoP verifies that our model can accurately reflect the polarization reflection properties of the target surface. In future work, we need to focus on the description at real swept angles and expect to progress our work in the field of rendering polarization properties of real-world materials.

Acknowledgment

This paper was produced by the IEEE Publication Technology Group. They are in Piscataway, NJ.

References

[1] J. M. Romano, D. Rosario, and J. McCarthy, "Day/night polarimetric anomaly detection using spice imagery," *IEEE Trans. Geosci. Remote Sens.*, vol. 50, no. 12, pp. 5014–5023, Dec. 2012.

[2] J. Liu, J. Duan, Y. Hao, G. Chen, and H. Zhang, "Semantic-guided polarization image fusion method based on a dual-discriminator GAN," *Opt. Exp.*, vol. 30, no. 24, pp. 43601–43621, 2022.

[3] H.-Y. Tan, N. Wang, S. Li, M. Hong, X. Wang, and Y. Feng, "The reactive oxygen species in macrophage polarization: Reflecting its dual role in progression and treatment of human diseases," *Oxidative Med. Cellular Longevity*, vol. 2016, pp. 1–16, 2016.

[4] M. Putintseva, E. Aksenov, C. Korikov, and E. Velichko, "Non-invasive research of biological objects by the method of laser polarimetry," in *Proc. J. Phys.: Conf. Ser.*, 2018, vol. 1124, no. 3, Art. no. 031021.

[5] J. Xu, W. Qian, and Q. Chen, "Calculation model of scattering depolarization for camouflaged target detection system," *Optik*, vol. 158, pp. 341–348, 2018.

[6] B. Fu et al., "Polarization-driven camouflaged object segmentation via gated fusion," *Appl. Opt.*, vol. 61, no. 27, pp. 8017–8027, 2022.

[7] M. L. Myrick et al., "The kubelka-munk diffuse reflectance formula revisited," *Appl. Spectrosc. Rev.*, vol. 46, no. 2, pp. 140–165, 2011.

[8] S. D. Butler, S. E. Nauyoks, and M. A. Marciniak, "Comparison of microfacet BRDF model to modified Beckmann-Kirchhoff BRDF model for rough and smooth surfaces," *Opt. Exp.*, vol. 23, no. 22, pp. 29100–29112, 2015.

[9] W. Feng, J. Li, Q. Wei, and L. Chen, "A hybrid model of polarized BRDF for rough surfaces," *Infrared Phys. Technol.*, vol. 53, no. 5, pp. 336–341, 2010.

[10] O. Romanyuk et al., "Microfacet distribution function for physically based bidirectional reflectance distribution functions," *Proc. SPIE*, vol. 8698, pp. 132–135, 2013.

[11] K. E. Torrance and E. M. Sparrow, "Theory for off-specular reflection from roughened surfaces∗," *J. Opt. Soc. Amer.*, vol. 57, no. 9, pp. 1105–1114, 1967.

[12] R. L. Cook and K. E. Torrance, "A reflectance model for computer graphics," *ACM Siggraph Comput. Graph.*, vol. 15, no. 3, pp. 307–316, 1981.

[13] A. Abrashuly and C. Valagiannopoulos, "Limits for absorption and scattering by core-shell nanowires in the visible spectrum," *Phys. Rev. Appl.*, vol. 11, no. 1, 2019, Art. no. 014051.

[14] M. W. Hyde IV, J. D. Schmidt, and M. J. Havrilla, "A geometrical optics polarimetric bidirectional reflectance distribution function for dielectric and metallic surfaces," *Opt. Exp.*, vol. 17, no. 24, pp. 22138–22153, 2009.

[15] R. G. Priest and T. A. Gerner, "Polarimetric BRDF in the microfacet model: Theory and measurements," in *Proc. Meeting Mil. Sens. Symposia Specialty Group Passive Sensors, Infrared Inf. Anal. Center*, 2000, vol. 1, pp. 169–181.

[16] H. Zhan and D. G. Voelz, "Modified polarimetric bidirectional reflectance distribution function with diffuse scattering: Surface parameter estimation," *Proc. SPIE*, vol. 55, no. 12, 2016, Art. no. 123103.

[17] C. Kulla and A. Conty, "Revisiting physically based shading at imageworks," *SIGGRAPH Course Physically Based Shading*, vol. 2, no. 3, 2017.

[18] J. H. Lee, A. Jarabo, D. S. Jeon, D. Gutierrez, and M. H. Kim, "Practical multiple scattering for rough surfaces," *ACM Trans. Graph.*, vol. 37, no. 6, pp. 1–12, 2018.

[19] V. Arellano, D. Gutierrez, and A. Jarabo, "Fast back-projection for non-line of sight reconstruction," in *Proc. ACM SIGGRAPH Posters*, 2017, pp. 1–2.

[20] M. Mojzik, T. Skrivan, A. Wilkie, and J. Krivanek, "Bi-directional polarised light transport," in *Proc. Eurograph. Symp. Rendering*, 2016, pp. 97–108.

[21] S.-H. Baek, D. S. Jeon, X. Tong, and M. H. Kim, "Simultaneous acquisition of polarimetric SVBRDF and normals," *ACM Trans. Graph.*, vol. 37, no. 6, 2018, Art. no. 268.

[22] Z. Cui, J. Gu, B. Shi, P. Tan, and J. Kautz, "Polarimetric multi-view stereo," in *Proc. IEEE Conf. Comput. Vis. Pattern Recognit.*, 2017, pp. 1558–1567.

[23] L. B. Wolff, S. K. Nayar, and M. Oren, "Improved diffuse reflection models for computer vision," *Int. J. Comput. Vis.*, vol. 30, pp. 55–71, 1998.

[24] J. Zhu, K. Wang, H. Liu, B. Du, and F. Guo, "Modified model of polarized bidirectional reflectance distribution function for metallic surfaces," *Opt. Laser Technol.*, vol. 99, pp. 160–166, 2018.

[25] J. Sun, X. Zhou, Z. Fan, and Q. Wang, "Investigation of light scattering properties based on the modified Li-Liang BRDF model," *Infrared Phys. Technol.*, vol. 120, 2022, Art. no. 103992.

[26] F. E. Nicodemus, "Reflectance nomenclature and directional reflectance and emissivity," *Appl. Opt.*, vol. 9, no. 6, pp. 1474–1475, 1970.

[27] K. P. Gurton and R. Dahmani, "Effect of surface roughness and complex indices of refraction on polarized thermal emission," *Appl. Opt.*, vol. 44, no. 26, pp. 5361–5367, 2005.

[28] M. Yang et al., "Degree of polarization modeling based on modified microfacet PBRDF model for material surface," *Opt. Commun.*, vol. 453, 2019, Art. no. 124390.

[29] S.-H. Baek and F. Heide, "Polarimetric spatio-temporal light transport probing," *ACM Trans. Graph.*, vol. 40, no. 6, pp. 1–18, 2021.

[30] Y. Kondo, T. Ono, L. Sun, Y. Hirasawa, and J. Murayama, "Accurate polarimetric BRDF for real polarization scene rendering," in *Proc. Comput. Vis.–ECCV: 16th Eur. Conf.*, 2020, pp. 220–236.

[31] S.-H. Baek et al., "Image-based acquisition and modeling of polarimetric reflectance," *ACM Trans. Graph.*, vol. 39, no. 4, 2020, Art. no. 139.

[32] P. Wang, P. Wang, F. Wang, S. Ye, and X. Wang, "Modified model of polarized bidirectional reflectance distribution function on material surface," *Acta Photonica Sinica*, vol. 48, no. 1, 2019, Art. no. 0126001.

[33] X. Li and Y. Liang, "Surface characteristics modeling and performance evaluation of urban building materials using LiDAR data," *Appl. Opt.*, vol. 54, no. 15, pp. 4750–4759, 2015.

[34] K. Wang, J.-P. Zhu, and H. Liu, "Degree of polarization based on the three-component pBRDF model for metallic materials," *Chin. Phys. B*, vol. 26, no. 2, 2017, Art. no. 024210.

[35] H. Shi, Y. Liu, C. He, C. Wang, Y. Li, and Y. Zhang, "Analysis of infrared polarization properties of targets with rough surfaces," *Opt. Laser Technol.*, vol. 151, 2022, Art. no. 108069.